Molecular Pharmacology Fast Forward. Published on October 28, 2014 as DOI: 10.1124/mol.114.094557
This article has not been copyedited and formatted. The final version may differ from this version.

Extracellular Surface Residues of the α_{1B}-Adrenoceptor Critical for GPCR Function

Lotten Ragnarsson, Åsa Andersson, Walter G. Thomas and Richard J. Lewis

Institute for Molecular Bioscience (LR, ÅA, RJL) and School of Biomedical Sciences (WGT), The University of Queensland, Brisbane, QLD 4072, Australia

Molecular Pharmacology Fast Forward. Published on October 28, 2014 as DOI: 10.1124/mol.114.094557
This article has not been copyedited and formatted. The final version may differ from this version.

RUNNING TITLE PAGE

GPCR extracellular surface function

To whom correspondence should be addressed: Richard J. Lewis, University of Queensland, Institute for Molecular Bioscience, Brisbane, Queensland 4072, Australia, Tel.: +61(0)7 3346 2984; E-mail: r.lewis@imb.uq.edu.au

Text pages: 12

Number of tables: 1

Number of figures: 8

References: 63

Number of words in the Abstract: 234

Number of words in the Introduction: 683

Number of words in the Discussion: 1663

α_{1B}-AR, α_{1B}-adrenoceptor; ECL, extracellular loop; ECS, extracellular surface; GPCR, G protein-coupled receptor; HEAT,(±)β-(iodo-4-hydroxyphenyl)-ethyl-aminomethyl-tetralone; HTRF, homogeneous time-resolved fluorescence; IP_1, inositol 1-phosphate; NE, norepinephrine; PDB, Protein Data Bank; SNP, single nucleotide polymorphism; TMH, transmembrane helix

Molecular Pharmacology Fast Forward. Published on October 28, 2014 as DOI: 10.1124/mol.114.094557
This article has not been copyedited and formatted. The final version may differ from this version.

ABSTRACT

Ligand binding and conformational changes that accompany signaling from G protein-coupled receptors (GPCRs) have mostly focused on the role of transmembrane helices (TMHs) and intracellular loop regions. However, recent studies, including several GPCRs co-crystallized with bound ligands, clearly show that the extracellular surface (ECS) of GPCRs plays an important role in ligand recognition, selectivity and binding, as well as potentially contributing to receptor activation and signaling. This study applied alanine-scanning mutagenesis to investigate the role of the complete extracellular surface (ECS) of the α_{1B}-AR on norepinephrine (NE) potency, affinity and efficacy. Half (24 of 48) of the ECS mutations significantly decreased NE potency in an IP-one assay. Most mutations reduced NE affinity (17) determined from ^{3}H-prazosin displacement studies, while four mutations at the entrance to the NE binding pocket enhanced NE affinity. Removing the influence of NE affinity and receptor expression levels on NE potency gave a measure of NE efficacy, which was significantly decreased for 11 of 48 ECS mutants. These different effects tended to cluster to different regions of the ECS, consistent with different regions of the ECS playing discrete functional roles. Exposed ECS residues at the entrance to the NE binding pocket mostly affected NE affinity, while buried or structurally significant residues mostly affected NE efficacy. The broad potential for ECS mutations to affect GPCR function has relevance for the increasing number non-synonymous single nucleotide polymorphisms now being identified in GPCRs.

Molecular Pharmacology Fast Forward. Published on October 28, 2014 as DOI: 10.1124/mol.114.094557
This article has not been copyedited and formatted. The final version may differ from this version.

INTRODUCTION

GPCRs regulate major physiological functions by coupling extracellular stimuli from hormones and neurotransmitters, and sensory stimuli from light, odorants and flavors, to intracellular signaling (Rosenbaum et al., 2009). The structure-function of GPCRs are regulated by highly conserved motifs in the TMHs, including the "ionic lock" between the highly conserved E/DRY motif on TMH3 and a glutamate residue on TMH6, the NPXXY motif at the cytoplasmic end of TMH7, and the "rotamer toggle switch" tryptophan in TMH6, that influence receptor transitions between the active and inactive states (Kobilka and Deupi, 2007; Rosenbaum et al., 2009; Granier and Kobilka, 2012; Venkatakrishnan et al., 2013). In addition, the recent crystal structure of the agonist-bound active state of the β_2-AR coupled to G_s reveals dynamic aspects of the cytoplasmic loops that are also critical for GPCR function (Rasmussen et al., 2011). Recent structures of active state GPCRs, including the β_2-AR, rhodopsin and the M2 muscarinic acetylcholine receptor (Rasmussen et al., 2011; Rosenbaum et al., 2011; Standfuss et al., 2011; Kruse et al., 2013; Venkatakrishnan et al., 2013) suggest the ECLs also contribute to ligand affinity and activation mechanisms, whereas the role of the ECS residues on GPCR structure-function has been largely overlooked (Nobles et al., 2011; Hu et al., 2013).

The α_{1B}-ARs belong to Class A GPCRs, the largest and most extensively characterized GPCRs of the rhodopsin-like receptor family. The growing number of crystal structures of bovine rhodopsin (Palczewski et al., 2000; Standfuss et al., 2011), bovine opsin (Park et al., 2008; Scheerer et al., 2008), human β_2-adrenergic (Cherezov et al., 2007; Rasmussen et al., 2011; Rosenbaum et al., 2011), turkey β_1-adrenergic (Warne et al., 2008), human A_{2A}-adenosine (Jaakola et al., 2008), human dopamine D3 (Chien et al., 2010), and human muscarinic M2 (Haga et al., 2012; Kruse et al., 2013) and rat M3 (Kruse et al., 2012) receptors now allow rational structure-based drug design and accurate modeling of other Class A GPCRs (Katritch et al., 2012; Matsoukas et al., 2013; Ragnarsson et al., 2013; Rodriguez and Gutierrez-de-Teran, 2013; Shim et al., 2013; Stevens et al., 2013). However, except for a conserved disulfide bond that connects a cysteine residue in ECL2 and

Molecular Pharmacology Fast Forward. Published on October 28, 2014 as DOI: 10.1124/mol.114.094557
This article has not been copyedited and formatted. The final version may differ from this version.

a cysteine residue located at the extracellular end of TMH3 critical for receptor folding and cell surface expression (Zeng et al., 1999), the ECLs are poorly conserved (Vaidehi et al., 2014). For example, the ECL2 in rhodopsin forms a short β-sheet that caps the covalently bound 11-cis-retinal, ECL2 in β_1- and β_2-ARs forms a short α-helix, whereas ECL2 in the A_{2A}-adenosine receptor lacks a defined secondary structure. Our model of the hamster α_{1B}-AR, built from the crystal structure of the turkey β_1-AR (PDB code 2VT4 (Warne et al., 2008), predicts a highly ordered ECL2 with several intramolecular interactions, a salt-bridge and a conserved disulfide bond, but no well-defined secondary structure (Ragnarsson et al., 2013). Interestingly, breaking this structurally important disulfide bond facilitated binding of the α_{1B}-AR selective allosteric antagonist ρ-TIA, despite reducing NE potency, affinity and efficacy (Ragnarsson et al., 2013).

Mechanistic insight into how conformational changes in the ECS can influence movement in the TMHs, and thus impact on activation and intracellular signaling, is important to fully understand the GPCR activation process and will facilitate the rational design of state-dependent GPCR modulators. Recent NMR studies of rhodopsin activation have shown that the ECL2 is displaced from the retinal binding site as a consequence of rearrangements in the hydrogen-bond network connecting ECL2 with the extracellular ends of TMH4, 5 and 6. Together with a movement of TMH5, which breaks the highly conserved ionic lock (E/DRY), these conformational shifts cause receptor activation (Ahuja et al., 2009). In addition, NMR studies of the β_2-AR have revealed that agonists and antagonists stabilize distinct GPCR conformations, demonstrating conformational coupling between the ECS and the orthosteric binding site (Bokoch et al., 2010). To investigate in detail how the ECS contributes to GPCR function, we systematically mutated all ECS residues of the α_{1B}-AR to alanine. This study revealed a surprisingly broad contribution of the ECS to function, with the majority of residues in ECL1 and ECL2 affecting NE potency and/or affinity at the α_{1B}-AR.

MATERIALS AND METHODS

Site-directed Mutagenesis

Molecular Pharmacology Fast Forward. Published on October 28, 2014 as DOI: 10.1124/mol.114.094557
This article has not been copyedited and formatted. The final version may differ from this version.

Professor R.M. Graham (Victor Chang Cardiac Research Institute, Sydney, Australia) kindly provided the hamster α_{1B}-AR cDNA in the pMT2' vector. The α_{1B}-AR subunit cDNA was subjected to *In vitro* site-directed mutagenesis using the QuikChangeTM mutagenesis kit (Stratagene) following the manufacturer's instructions. The following point mutations in the α_{1B}-AR were created: V107A, L108A, G109A, Y110A, W111A, V112A, L113A, G114A, R115A, I116A, C118A, P180A, L181A, L182A, G183A, W184A, K185A, E186A, P187A, P189A, N190A, D191A, D192A, K193A, E194A, C195A, G196A, V197A, T198A, E199A, E200A, P201A, F202A, L316A, G317A, S318A, S319A, F320A, S321A, T322A, L323A, K324A, P325A, P326A, D327A, V329A, F330A and K331A. Primers used to generate the mutants were from Sigma-Aldrich. *TOP10 Escherichia coli* (Invitrogen) were transformed with wild type (WT) and mutant cDNA and subsequently used for plasmid preparation using a PureLink® Quick Plasmid Miniprep Kit (Invitrogen) or High Speed Maxi kit (Qiagen). Purified cDNA was used to confirm all mutations by sequencing by the Australian Genome Research Facility.

Transient expression of α_{1B}-ARs and membrane preparation

The transient expression of α_{1B}-ARs and the membrane preparations were performed as described previously (Ragnarsson et al., 2013). To assess the influence of expression levels on NE potency, we transfected WT α_{1B}-AR with reduced DNA levels (0.3, 0.1 and 0.03 of our standard 6 µg DNA per T25 flask) and determined NE EC_{50}, E_{max} and K_A using the IP-one HTRF assay, and B_{max} from bound levels of a K_d concentration of ^{3}H-prazosin (0.5 nM).

Radioligand binding assays

Saturation binding experiments were performed as described before to determine the B_{max} and prazosin K_d at each of the mutants (Ragnarsson et al., 2013). Briefly, membranes from α_{1B}-AR-transfected COS-1 cells (5 µg protein) were incubated with increasing concentrations of ^{3}H-prazosin (5 pM–5 nM) for 60 min at room temperature. Non-specific binding was determined in the presence of 10 µM phentolamine. The affinity of NE at the α_{1B}-AR mutants were determined using the

Molecular Pharmacology Fast Forward. Published on October 28, 2014 as DOI: 10.1124/mol.114.094557
This article has not been copyedited and formatted. The final version may differ from this version.

radiolabelled α_1-AR antagonist ^{3}H-prazosin (0.5 nM) or ^{125}I-(±)β-(iodo-4-hydroxyphenyl)-ethyl-aminomethyl-tetralone (^{125}I-HEAT; 70 pM) for the C195A mutant. Reactions containing radioligand, membranes from α_{1B}-AR-transfected COS-1 cells (5 µg protein) and eight NE concentrations (1 nM–10 mM) in HEM buffer, were established in clear round bottom 96 well plates. Each experiment was performed in triplicate in a total reaction volume of 150 µL. After incubation for 60 min at room temperature the membranes were harvested onto Whatman GF/B filtermats (PerkinElmer) pre-treated with 0.6% polyethylenimine using a Tomtec harvester. BetaPlate scintillant (PerkinElmer) was added and the filter-bound radioactivity detected using a Wallac MicroBeta (PerkinElmer).

IP-one HTRF assay

The IP-one HTRF assay was performed as previously described (Ragnarsson et al., 2013).

Molecular Modeling

A molecular homology model of the α_{1B}-AR (Data Supplement 1) was built using the crystal structure of the turkey β_1-adrenoceptor (PDB code 2VT4) as previously described (Ragnarsson et al., 2013).

Statistics and Data Analysis

Sigmoidal curves for the calculation of the half-maximal excitatory concentration (EC_{50}) were fitted to individual data points by non-linear regression using the software package Prism (GraphPad Software). The maximum agonist response (E_{max}) was calculated as the difference between the maximal and minimal response to NE, and presented as percent of maximal WT response on the day of the assay for normalization. The NE signaling efficiency (NE efficacy) was calculated as the NE pEC_{50} value minus the NE K_i value, with additional adjustment for the significantly reduced expression levels (observed only for the C118A mutant). B_{max} values determined from two 12-point saturation binding experiments with 95% confidence intervals overlapping WT values were

Molecular Pharmacology Fast Forward. Published on October 28, 2014 as DOI: 10.1124/mol.114.094557
This article has not been copyedited and formatted. The final version may differ from this version.

considered not significantly different from WT, otherwise these experiments were performed in triplicate.

An operational model was fitted to the NE concentration response curves for the IP_1 accumulation assay to examine the influence of four levels of α_{1B}-AR expression on NE EC_{50}, affinity and efficacy using Prism (GraphPad Software). The operational model generates a global estimate of the functional dissociation constant (K_A) for NE. This model also takes into consideration agonist efficacy (τ), the inverse of the fraction of receptors occupied by NE that produce the half-maximal response (i.e. τ = 10 indicates only 10% of the receptors need to be activated to produce a half-maximal response).

For multiple comparisons, one-way ANOVA was used with post-hoc *t*-tests performed by Dunnett's method, using Prism (GraphPad Software). Values of $P < 0.05$ were considered significant. The ANOVA on EC_{50}, K_i and efficacy data was performed on the log values.

RESULTS

Prazosin affinity (K_d) and B_{max} at ECS mutants of the α_{1B}-AR

Prazosin binds in the orthosteric pocket below the ECS of the α_{1B}-AR (Ragnarsson et al., 2013), and was used to evaluate the expression levels and structural integrity of the 48 ECS mutants (Fig. 1, Table 1). In ECL1, G109A and G114A showed a significant 9- and 8-fold increase in prazosin affinity compared to WT, as reported previously (Ragnarsson et al., 2013). There was no change in prazosin K_d for the mutants in the TMHs adjoining ECL1; TMH2 and TMH3. In ECL2, no mutants significantly affected prazosin K_d, but in the adjoining TMH4, the G183A mutant significantly decreased prazosin affinity (4-fold) (Ragnarsson et al., 2013). In contrast, alanine mutations in ECL3 and the ECS residues in adjoining TMH6 and 7 had no significant effect on prazosin affinity. B_{max} values were generated for all mutants, with only the C118A mutant showing reduced expression at 11% of WT levels (Table 1).

Molecular Pharmacology Fast Forward. Published on October 28, 2014 as DOI: 10.1124/mol.114.094557
This article has not been copyedited and formatted. The final version may differ from this version.

Signaling of α_{1B}-AR ECS mutants in response to NE

To fully characterize the role of the highly variable ECS of the α_{1B}-AR on signaling, mutations to alanine at each position in the extended ECS were made and the effect on NE signaling to IP_1 determined (Fig. 2, Table 1), a downstream metabolite of IP_3 that accumulates in cells following G_q activation. In ECL1, NE had significantly reduced potency at the Y110A, W111A, L113A, G114A and R115A mutants in ECL1 (3-, 11-, 12-, 16- and 10-fold, respectively) compared with WT receptor (EC_{50} = 11.9 ± 0.58 nM) (Fig. 2, Table 1). In the adjoining TMH3, the C118A mutant (cysteine partner to C195 in ECL2) decreased NE potency 937-fold compared with WT (Fig. 2, Table 1). After adjusting the C118A EC_{50} for the lower B_{max} (~ 11% of WT), a significant 103-fold decrease in potency compared to WT was still observed. In ECL2, NE had significantly decreased potency at the W184A, K185A, E186A, P189A, N190A, D191A, C195A, G196A, V197A, T198A and E200A mutants compared with WT (33-, 26-, 13-, 5-, 40-, 4-, 1486-, 10-, 6-, 20- and 20-fold change, respectively). ECL2 adjoins TMH4 and TMH5, and while the NE potency was unaffected by ECS mutations in TMH5, the P180A, L181A and G183A mutants in TMH4 decreased NE potency 335-, 20- and 276-fold, respectively, compared with WT receptor (Fig. 2, Table 1). In contrast, only the P326A mutation in ECL3 caused a small but significant 3-fold change in NE potency compared to WT. In the adjoining TMH6, only the G317A mutant decreased NE potency 4-fold compared with WT, and no changes were observed for mutations in TMH7 (Fig. 2, Table 1).

Characterization of the efficacy of NE at ECS mutants of the α_{1B}-AR

The maximal response (E_{max}) to NE was determined at the ECS mutants and compared with the WT α_{1B}-AR response on the day of assay to determine NE efficacy. Only one of the alanine mutants constructed (C118A α_{1B}-AR) significantly altered the efficacy of NE, reducing responses to 53% of WT (Table 1). We saw no indication of any increased basal activities for any of the mutants tested that would be indicative of a constitutively active mutant.

NE affinity (K_i) at ECS mutants of the α_{1B}-AR

Molecular Pharmacology Fast Forward. Published on October 28, 2014 as DOI: 10.1124/mol.114.094557
This article has not been copyedited and formatted. The final version may differ from this version.

The NE affinity (K_i) was determined for all the ECS mutants to evaluate their effect on NE binding (Fig. 3 and Table 1). In ECL1, NE had significantly decreased affinity at the W111A and R115A receptor mutants (6- and 2-fold, respectively), whereas the G109A receptor mutant had 3-fold increased NE affinity compared with WT receptor (K_i = 19.50 ± 1.83 μM; *n* = 10) (Fig. 3, Table 1). In the adjoining TMHs, the α_{1B}-AR mutant V107A in TMH2 increased the NE affinity 2-fold compared with WT, whereas the C118A mutant in TMH3 decreased the NE affinity 26-fold compared with WT (Fig. 3, Table 1).

In ECL2, NE had significantly decreased affinity at the W184A, K185A, E186A, N190A, D191A, D192A, C195A, T198A and E200A mutants compared with WT (18-, 9-, 6-, 4-, 3-, 2-, 176-, 11- and 5-fold change, respectively). The P180A, L181A and G183A mutants in TMH4 adjacent to ECL2 decreased NE affinity (22-, 3- and 123-fold, respectively) compared with WT, while the NE potency was unaffected by ECL2-adjoining residues in TMH5 (Fig. 3, Table 1).

In ECL3, only the L323A mutation in ECL3 caused a significant 2-fold decrease in NE affinity compared to WT receptor. Of the adjoining ECS residues in TMH6, only the G317A mutant decreased NE affinity 3-fold compared with WT, whereas the F330A and K331A mutants in the ECS of TMH7 increased the NE affinity (3- and 9-fold, respectively) compared with WT (Fig. 3, Table 1).

NE signaling efficiency (NE efficacy) of α_{1B}-AR ECS mutants in response to NE

To characterize how effectively NE activated WT and mutant receptors, we removed the influence of NE affinity (pK_i) on NE potency (pEC_{50}) to obtain a measure of efficacy (NE efficacy = pEC_{50} – pK_i). From this assessment, only 2 mutants in ECL1 (L113A and G114A) had significantly reduced NE signaling efficiency (9- and 18-fold, respectively) compared with WT NE efficacy (3.22 ± 0.14, *n* = 10) (Fig. 4). In ECL2, 4 mutants (N190A, C195A, G196A and V197A) showed reduced efficacy (10-, 8-, 7- and 12-fold, respectively) compared with WT (Fig. 4). In contrast, no ECL3 mutants affected NE efficacy. In the adjoining TMHs, C118A in TMH3 had a 35-fold reduced NE efficacy after adjusting for significantly reduced expression, and in TMH4 the P180A and L181A receptor

Molecular Pharmacology Fast Forward. Published on October 28, 2014 as DOI: 10.1124/mol.114.094557
This article has not been copyedited and formatted. The final version may differ from this version.

mutants showed a 15- and 6-fold reduction in efficacy, respectively. In TMH7, the F330A and K331A mutants showed a 9- and 7-fold decrease in NE efficacy, respectively.

The influence of expression levels on NE potency

To investigate the influence of receptor density on NE pharmacology, we transfected with four different levels of WT α_{1B}-AR and fitted to an operational model to the NE concentration response curves from the IP_1 accumulation data using Prism (GraphPad Software) (Fig. 5). The operational model gave a global measure of NE functional affinity (pK_A = 6.94 ± 0.33 M, *n* = 3). We also plotted log(τ) against the corresponding log(B_{max}) values, which were significant (r^2 = 0.67) fitted by a linear regression with a slope of 1.8 ± 0.4 (Fig. 5 inset). These data confirm that the levels of WT α_{1B}-AR expression used in this study (1x) generated maximal NE responses (τ > 10). NE affinity determined from the IP-one experiments using the operational model was significantly lower (>100-fold) than the K_i measured from displacement of ^{3}H-prazosin binding to cell membrane preparations (pK_i = 4.71 ± 0.09 M, *n* = 10). ^{3}H-prazosin displacement studies performed on intact whole cells expressing the α_{1B}-AR showed comparable NE affinity to the binding data obtained from membranes made from transfected cells (pK_i 4.09 ± 0.16 M, *n* = 4).

DISCUSSION

To investigate how ECS residues contribute to function in Class A GPCRs, we performed a systematic alanine scan of the complete ECS of the α_{1B}-AR (Fig. 1) and identified residues that contributed to NE potency, affinity and/or signaling efficacy. This study revealed that the majority of ECL1 and ECL2 residues and one ECL3 residue, plus a number of ECS residues associated with TMHs, contributed significantly to α_{1B}-AR affinity and/or efficacy (Fig. 6). Many of the functionally significant ECS residues either lined the entrance to the NE binding pocket, where they might affect NE access, or lay outside the entrance where they might allosterically modulate NE function. Together, these data support the view that the ECS of GPCRs not only provides a path to the ligand binding pocket but also contributes to receptor activation (Ahuja et al., 2009; Ring et al., 2013).

Molecular Pharmacology Fast Forward. Published on October 28, 2014 as DOI: 10.1124/mol.114.094557
This article has not been copyedited and formatted. The final version may differ from this version.

Previous studies have revealed a number of ECL1 residues that influence receptor activation (Hawtin et al., 2006; Clark et al., 2010; Peeters et al., 2011), including the structurally important WXFG motif common to Class A GPCRs (Klco et al., 2006). The α_{1B}-AR has a related WVLG motif in ECL1, where the W111A mutant reduced NE potency without affecting efficacy, while the L113A and G114A reduced efficacy without affecting potency. In addition, the adjoining ECL1 mutant Y110A also reduced potency but not efficacy, whereas R115A reduced NE affinity but not efficacy. These residues are positioned outside the entrance to the NE binding pocket, consistent with the WVLG motif also playing a structural role in the α_1-adrenoceptor. ECL1 adjoins TMH3 and shares conserved interhelical interfaces with all other TMHs except THM1 and TMH7. ECL1 is thus considered critical in maintaining the structural scaffold of Class A GPCRs (Venkatakrishnan et al., 2013) and mutations in ECL1 that affect affinity and efficacy presumably distort the ECS confirmation and influence this equilibrium. This is supported by data from the C118A mutation in TMH3, which breaks the disulfide bond to C195 in ECL2, leading to decreased expression and the largest reductions in NE potency arising from reductions in both NE affinity and efficacy. In addition, ECL2 in our model is connected to ECL1 via two hydrogen bonds (W111 main chain to K193 main chain and R115 main chain to D192 side chain), which might contribute to the influence of these ECL1 mutations on NE affinity.

ECL2 is the most extensively studied and least conserved extracellular loop in GPCRs, both in terms of sequence and structure. In rhodopsin, ECL2 folds into the transmembrane crevice and participates in the orthosteric binding site for retinal (Palczewski et al., 2000). ECL2 also contributes to dopamine binding to the D2 receptor (Shi and Javitch, 2004). A chimeric study of the human-rat $P2Y_4$ receptor revealed that ECL2 influenced agonist versus antagonist function (Herold et al., 2004) and point mutations in the ECL2 produced constitutively active receptors (Klco et al., 2005) or inhibitory effects on signaling when ECL2 flexibility was affected (Avlani et al., 2007). In ECL2 of the α_{1B}-AR, 11 of 16 mutants reduced NE potency, including nine that decreased NE affinity (W184A, K185A, E186A, N190A, D191A, D192A, C195A, T198A and E200A) and four that reduced NE efficacy (N190A, C195A, G196A and V197A). An earlier mutational study swapped

Molecular Pharmacology Fast Forward. Published on October 28, 2014 as DOI: 10.1124/mol.114.094557
This article has not been copyedited and formatted. The final version may differ from this version.

three of these residues in ECL2 of the α_{1B}-AR to the corresponding residue in the α_{1A}-AR (G196Q, V197I, T198N) and showed that these residues influenced antagonist selectivity between these subtypes (Hwa et al., 1995; Zhao et al., 1996). Examining our model of the α_{1B}-AR, these three ECL2 residues are positioned where they might influence how NE reaches the orthosteric site in the α_{1B}-AR (see Fig. 6 and 7).

In our model of the α_{1B}-AR (Ragnarsson et al., 2013), ECL2 is stabilized by several intramolecular interactions in addition to being anchored to the extracellular end of TMH3 via a conserved cysteine bond that may promote stabilization of the inactive state (Massotte and Kieffer, 2005). Thus, is it not surprising that breaking the conserved disulfide bond bridging ECL2 to TMH3 in the C118A and C195A mutants had a dramatic effect on agonist potency, as shown previously for the α_{1B}-AR (Ragnarsson et al., 2013) and other Class A GPCRs (Dixon et al., 1987; Karnik et al., 1988; Fraser, 1989; Dohlman et al., 1990; Karnik and Khorana, 1990; Kurtenbach et al., 1990; Noda et al., 1994; Perlman et al., 1995; Lin and Sakmar, 1996; Cook and Eidne, 1997; Zhou and Tai, 2000). The C118A and C195A mutants reduced both NE affinity and efficacy, indicating that this conserved disulfide bridge stabilizes a conformation that facilitates both NE access to its binding site and NE signaling. Mutations in TMH4 adjacent to ECL2 (P180A and L181A) and two residues adjacent to C195 (G196A and V197A) also reduced NE affinity and efficacy, supporting a scaffolding role for TMH4 that is critical for normal functioning of the α_{1B}-AR. Interestingly, the G183A mutant at the ECS of TMH4 had decreased prazosin and NE affinity, but unchanged efficacy, opposite to the effect seen for the G109A mutant in ECL1 (Ragnarsson et al., 2013).

In contrast to the majority of ECL1 and ECL2 mutations affecting α_{1B}-AR function, only L323A in ECL3 decreased NE affinity, while the K324A and P326A mutants associated with TMH7 significantly reduced NE potency. A minor role played by ECL3 in receptor activation is in agreement with results from a study on the adenosine A1 receptor (Peeters et al., 2012), while ECL3 was shown to be important for δ-opioid receptor (Decaillot et al., 2003) and β_2-AR activation (Zhao et al., 1998). Two mutations adjacent to ECL3 (F330 and K331A in TMH7) significantly enhanced

Molecular Pharmacology Fast Forward. Published on October 28, 2014 as DOI: 10.1124/mol.114.094557
This article has not been copyedited and formatted. The final version may differ from this version.

NE affinity but reduced NE efficacy without affecting prazosin affinity (Ragnarsson et al., 2013). In contrast, mutating the equivalent residue to F330 in the α_{1A}-AR (Phe308) had no effect on antagonist binding and either showed no effect or decreased agonist affinity depending on the agonist investigated (Waugh et al., 2001). A stabilizing salt bridge between D125 in TMH3 and K331 in TMH7 has been reported to maintain the inactive state of the receptor (Porter et al., 1996). Our α_{1B}-AR model does not form this salt bridge, although both the F330A and K331A mutants had increased NE affinity and reduced NE efficacy, suggesting a complex effect on NE function that appears independent of a salt-bridge effect. Interestingly, a phenylalanine at a position equivalent to F330 in the α_{1B}-AR is conserved in all adrenoceptors except the β_2-AR (see Fig. 7).

The effects of ECS mutations on NE affinity and/or efficacy tended to cluster in different regions of the ECS (Fig. 6B). Mutations that reduced NE affinity alone clustered at the start of ECL1, across most of ECL2 and at the start of ECL3, whereas mutations that reduced efficacy alone appeared in small clusters in the central portion of ECL1 and the second half of ECL2. In contrast, mutations likely to have structural effects, including C118A, P180A and C195A, had large effects on both affinity and efficacy, whereas mutations that enhanced NE affinity clustered at the TMH2-ECL1 and ECL3-TMH7 junctions, which are adjacent in GPCR structures. These results suggest that different regions of the ECS play discrete roles in GPCR function. Depending on position, mutating hydrophobic, polar and charged residues to alanine all contributed to changed function. A functional heat map of the ECS (Fig. 7) revealed that residues lining the upper lip of the entrance to the NE binding pocket reduced NE affinity, while mutating residues lining the lower lip mostly enhanced NE affinity. Given these residues line the entrance to the NE binding pocket they likely directly influence NE binding kinetics. In contrast, relatively few exposed residues greatly affected NE efficacy (mostly <10-fold), whereas buried or structurally significant residues tended to have more significant effects on NE efficacy.

Figure 8 shows sequence alignments for the ECS residues of hamster α_{1B}-AR and selected Class A GPCRs, including human α_{1B}-AR, α_{1A}-AR, α_{1D}-AR, α_{2A}-AR, β_1-AR, β_2-AR, muscarinic M2 and M3

receptor, dopamine D3 receptor, histamine H1 receptor and κ-opioid receptors. This alignment reveals that many of the residues in and adjoining ECL1 are conserved, while residues in ECL2 and ECL3 are less conserved. Interestingly, superimposing our mutational results on this alignment revealed that most of the functionally significant mutations are positioned in the more conserved regions of the ECS, especially in the highly conserved ECL1 (Fig. 8). The broad potential for ECS mutations to affect GPCR function has relevance for the increasing number non-synonymous single nucleotide polymorphisms (SNPs) now being identified in GPCRs through next generation sequencing (Hecht et al., 2013). SNPs have the potential to alter receptor pharmacology and response to medication and can predispose people to various diseases (Thompson et al., 2008). SNPs of potential medical importance have been identified at the ECS of aminergic GPCRs (Kojima et al., 2009), including R166K in the human α_{1A}-AR, which reduced both NE affinity and potency in rat fibroblasts (Lei et al., 2005). Interestingly, this position corresponds to K185 in ECL2 of the α_{1B}-AR, which also significantly decreased NE potency and NE affinity when mutated to alanine, showing a potential conserved structural role for this residue. Another ECS SNP identified in the histamine H1 receptor (L449S corresponding to V329 in TMH7 of the hamster α_{1B}-AR) was suspected of being involved in asthma. However, no correlation to asthma was identified (Mancama et al., 2002), consistent with the lack of effect of the V329A mutation on α_{1B}-AR function.

In conclusion, this study reveals that mutating ECS residues of GPCRs can have profound effects on agonist affinity and/or efficacy. At the α_{1B}-AR, the type of effect produced clustered to different regions of the ECS, consistent with different regions of the ECS playing discrete functional roles. Collectively, our data highlight that changes in NE potency result from effects on NE affinity mostly though more conserved regions of ECL1 and ECL2 that surround the entrance to the NE binding pocket or are associated with the ECS of TMH4 and TMH7, or from effects on signaling efficacy mostly through buried or structurally significant residues.

Molecular Pharmacology Fast Forward. Published on October 28, 2014 as DOI: 10.1124/mol.114.094557
This article has not been copyedited and formatted. The final version may differ from this version.

AUTHORSHIP CONTRIBUTION

Participated in research design: Ragnarsson, Andersson, Thomas and Lewis

Conducted experiments: Ragnarsson and Andersson

Contributed new reagents or analytical tools: N/A

Performed data analysis: Ragnarsson, Andersson and Lewis

Wrote or contributed to the writing of the manuscript: Ragnarsson, Thomas and Lewis

Molecular Pharmacology Fast Forward. Published on October 28, 2014 as DOI: 10.1124/mol.114.094557
This article has not been copyedited and formatted. The final version may differ from this version.

REFERENCES

Ahuja S., Hornak V., Yan E.C., Syrett N., Goncalves J.A., Hirshfeld A., Ziliox M., Sakmar T.P., Sheves M., Reeves P.J., Smith S.O. and Eilers M. (2009) Helix movement is coupled to displacement of the second extracellular loop in rhodopsin activation. *Nat Struct Mol Biol* **16**, 168-75.

Avlani V.A., Gregory K.J., Morton C.J., Parker M.W., Sexton P.M. and Christopoulos A. (2007) Critical role for the second extracellular loop in the binding of both orthosteric and allosteric G protein-coupled receptor ligands. *J Biol Chem* **282**, 25677-86.

Bokoch M.P., Zou Y., Rasmussen S.G., Liu C.W., Nygaard R., Rosenbaum D.M., Fung J.J., Choi H.J., Thian F.S., Kobilka T.S., Puglisi J.D., Weis W.I., Pardo L., Prosser R.S., Mueller L. and Kobilka B.K. (2010) Ligand-specific regulation of the extracellular surface of a G-protein-coupled receptor. *Nature* **463**, 108-12.

Cherezov V., Rosenbaum D.M., Hanson M.A., Rasmussen S.G., Thian F.S., Kobilka T.S., Choi H.J., Kuhn P., Weis W.I., Kobilka B.K. and Stevens R.C. (2007) High-resolution crystal structure of an engineered human β2-adrenergic G protein-coupled receptor. *Science* **318**, 1258-65.

Chien E.Y., Liu W., Zhao Q., Katritch V., Han G.W., Hanson M.A., Shi L., Newman A.H., Javitch J.A., Cherezov V. and Stevens R.C. (2010) Structure of the human dopamine D3 receptor in complex with a D2/D3 selective antagonist. *Science* **330**, 1091-5.

Clark S.D., Tran H.T., Zeng J. and Reinscheid R.K. (2010) Importance of extracellular loop one of the neuropeptide S receptor for biogenesis and function. *Peptides* **31**, 130-8.

Cook J.V. and Eidne K.A. (1997) An intramolecular disulfide bond between conserved extracellular cysteines in the gonadotropin-releasing hormone receptor is essential for binding and activation. *Endocrinology* **138**, 2800-6.

Decaillot F.M., Befort K., Filliol D., Yue S., Walker P. and Kieffer B.L. (2003) Opioid receptor random mutagenesis reveals a mechanism for G protein-coupled receptor activation. *Nat Struct Biol* **10**, 629-36.

Dixon R.A., Sigal I.S., Candelore M.R., Register R.B., Scattergood W., Rands E. and Strader C.D. (1987) Structural features required for ligand binding to the beta-adrenergic receptor. *EMBO J* **6**, 3269-75.

Dohlman H.G., Caron M.G., DeBlasi A., Frielle T. and Lefkowitz R.J. (1990) Role of extracellular disulfide-bonded cysteines in the ligand binding function of the β2-adrenergic receptor. *Biochemistry* **29**, 2335-42.

Fraser C.M. (1989) Site-directed mutagenesis of beta-adrenergic receptors. Identification of conserved cysteine residues that independently affect ligand binding and receptor activation. *J Biol Chem* **264**, 9266-70.

Granier S. and Kobilka B. (2012) A new era of GPCR structural and chemical biology. *Nat Chem Biol* **8**, 670-3.

Haga K., Kruse A.C., Asada H., Yurugi-Kobayashi T., Shiroishi M., Zhang C., Weis W.I., Okada T., Kobilka B.K., Haga T. and Kobayashi T. (2012) Structure of the human M2 muscarinic acetylcholine receptor bound to an antagonist. *Nature* **482**, 547-51.

Hawtin S.R., Simms J., Conner M., Lawson Z., Parslow R.A., Trim J., Sheppard A. and Wheatley M. (2006) Charged extracellular residues, conserved throughout a G-protein-coupled receptor family, are required for ligand binding, receptor activation, and cell-surface expression. *J Biol Chem* **281**, 38478-88.

Hecht M., Bromberg Y. and Rost B. (2013) News from the protein mutability landscape. *J Mol Biol* **425**, 3937-48.

Herold C.L., Qi A.D., Harden T.K. and Nicholas R.A. (2004) Agonist versus antagonist action of ATP at the P2Y4 receptor is determined by the second extracellular loop. *J Biol Chem* **279**, 11456-64.

Hu J., Hu K., Liu T., Stern M.K., Mistry R., Challiss R.A., Costanzi S. and Wess J. (2013) Novel structural and functional insights into M3 muscarinic receptor dimer/oligomer formation. *J Biol Chem* **288**, 34777-90.

Hwa J., Graham R.M. and Perez D.M. (1995) Identification of critical determinants of α1-adrenergic receptor subtype selective agonist binding. *J Biol Chem* **270**, 23189-95.

Jaakola V.P., Griffith M.T., Hanson M.A., Cherezov V., Chien E.Y., Lane J.R., Ijzerman A.P. and Stevens R.C. (2008) The 2.6 angstrom crystal structure of a human A2A adenosine receptor bound to an antagonist. *Science* **322**, 1211-7.

Karnik S.S. and Khorana H.G. (1990) Assembly of functional rhodopsin requires a disulfide bond between cysteine residues 110 and 187. *J Biol Chem* **265**, 17520-4.

Karnik S.S., Sakmar T.P., Chen H.B. and Khorana H.G. (1988) Cysteine residues 110 and 187 are essential for the formation of correct structure in bovine rhodopsin. *Proc Natl Acad Sci U S A* **85**, 8459-63.

Katritch V., Cherezov V. and Stevens R.C. (2012) Diversity and modularity of G protein-coupled receptor structures. *Trends Pharmacol Sci* **33**, 17-27.

Klco J.M., Nikiforovich G.V. and Baranski T.J. (2006) Genetic analysis of the first and third extracellular loops of the C5a receptor reveals an essential WXFG motif in the first loop. *J Biol Chem* **281**, 12010-9.

Klco J.M., Wiegand C.B., Narzinski K. and Baranski T.J. (2005) Essential role for the second extracellular loop in C5a receptor activation. *Nat Struct Mol Biol* **12**, 320-6.

Kobilka B.K. and Deupi X. (2007) Conformational complexity of G-protein-coupled receptors. *Trends Pharmacol Sci* **28**, 397-406.

Kojima Y., Sasaki S., Hayashi Y., Tsujimoto G. and Kohri K. (2009) Subtypes of α1-adrenoceptors in BPH: future prospects for personalized medicine. *Nat Clin Pract Urol* **6**, 44-53.

Kruse A.C., Hu J., Pan A.C., Arlow D.H., Rosenbaum D.M., Rosemond E., Green H.F., Liu T., Chae P.S., Dror R.O., Shaw D.E., Weis W.I., Wess J. and Kobilka B.K. (2012) Structure and dynamics of the M3 muscarinic acetylcholine receptor. *Nature* **482**, 552-6.

Kruse A.C., Ring A.M., Manglik A., Hu J., Hu K., Eitel K., Hubner H., Pardon E., Valant C., Sexton P.M., Christopoulos A., Felder C.C., Gmeiner P., Steyaert J., Weis W.I., Garcia K.C., Wess J. and Kobilka B.K. (2013) Activation and allosteric modulation of a muscarinic acetylcholine receptor. *Nature*.

Kurtenbach E., Curtis C.A., Pedder E.K., Aitken A., Harris A.C. and Hulme E.C. (1990) Muscarinic acetylcholine receptors. Peptide sequencing identifies residues involved in antagonist binding and disulfide bond formation. *J Biol Chem* **265**, 13702-8.

Lei B., Morris D.P., Smith M.P., Svetkey L.P., Newman M.F., Rotter J.I., Buchanan T.A., Beckstrom-Sternberg S.M., Green E.D. and Schwinn D.A. (2005) Novel human α1a-adrenoceptor single nucleotide polymorphisms alter receptor pharmacology and biological function. *Naunyn Schmiedebergs Arch Pharmacol* **371**, 229-39.

Lin S.W. and Sakmar T.P. (1996) Specific tryptophan UV-absorbance changes are probes of the transition of rhodopsin to its active state. *Biochemistry* **35**, 11149-59.

Mancama D., Arranz M.J., Munro J., Osborne S., Makoff A., Collier D. and Kerwin R. (2002) Investigation of promoter variants of the histamine 1 and 2 receptors in schizophrenia and clozapine response. *Neurosci Lett* **333**, 207-11.

Massotte D. and Kieffer B.L. (2005) The second extracellular loop: a damper for G protein-coupled receptors? *Nat Struct Mol Biol* **12**, 287-8.

Matsoukas M.T., Cordomi A., Rios S., Pardo L. and Tselios T. (2013) Ligand binding determinants for angiotensin II type 1 receptor from computer simulations. *J Chem Inf Model* **53**, 2874-83.

Miao Y., Nichols S.E., Gasper P.M., Metzger V.T. and McCammon J.A. (2013) Activation and dynamic network of the M2 muscarinic receptor. *Proc Natl Acad Sci U S A* **110**, 10982-7.

Nobles K.N., Xiao K., Ahn S., Shukla A.K., Lam C.M., Rajagopal S., Strachan R.T., Huang T.Y., Bressler E.A., Hara M.R., Shenoy S.K., Gygi S.P. and Lefkowitz R.J. (2011) Distinct phosphorylation sites on the β2-adrenergic receptor establish a barcode that encodes differential functions of β-arrestin. *Sci Signal* **4**, ra51.

Noda K., Saad Y., Graham R.M. and Karnik S.S. (1994) The high affinity state of the β2-adrenergic receptor requires unique interaction between conserved and non-conserved extracellular loop cysteines. *J Biol Chem* **269**, 6743-52.

Palczewski K., Kumasaka T., Hori T., Behnke C.A., Motoshima H., Fox B.A., Le Trong I., Teller D.C., Okada T., Stenkamp R.E., Yamamoto M. and Miyano M. (2000) Crystal structure of rhodopsin: A G protein-coupled receptor. *Science* **289**, 739-45.

Park J.H., Scheerer P., Hofmann K.P., Choe H.W. and Ernst O.P. (2008) Crystal structure of the ligand-free G-protein-coupled receptor opsin. *Nature* **454**, 183-7.

Peeters M.C., van Westen G.J., Guo D., Wisse L.E., Muller C.E., Beukers M.W. and Ijzerman A.P. (2011) GPCR structure and activation: an essential role for the first extracellular loop in activating the adenosine A2B receptor. *FASEB J* **25**, 632-43.

Peeters M.C., Wisse L.E., Dinaj A., Vroling B., Vriend G. and Ijzerman A.P. (2012) The role of the second and third extracellular loops of the adenosine A1 receptor in activation and allosteric modulation. *Biochem Pharmacol* **84**, 76-87.

Perlman J.H., Wang W., Nussenzveig D.R. and Gershengorn M.C. (1995) A disulfide bond between conserved extracellular cysteines in the thyrotropin-releasing hormone receptor is critical for binding. *J Biol Chem* **270**, 24682-5.

Porter J.E., Hwa J. and Perez D.M. (1996) Activation of the α1b-adrenergic receptor is initiated by disruption of an interhelical salt bridge constraint. *J Biol Chem* **271**, 28318-23.

Ragnarsson L., Wang C.I., Andersson A., Fajarningsih D., Monks T., Brust A., Rosengren K.J. and Lewis R.J. (2013) Conopeptide ρ-TIA defines a new allosteric site on the extracellular surface of the α1B-adrenoceptor. *J Biol Chem* **288**, 1814-27.

Rasmussen S.G., DeVree B.T., Zou Y., Kruse A.C., Chung K.Y., Kobilka T.S., Thian F.S., Chae P.S., Pardon E., Calinski D., Mathiesen J.M., Shah S.T., Lyons J.A., Caffrey M., Gellman S.H., Steyaert J., Skiniotis G., Weis W.I., Sunahara R.K. and Kobilka B.K. (2011) Crystal structure of the β2 adrenergic receptor-Gs protein complex. *Nature* **477**, 549-55.

Ring A.M., Manglik A., Kruse A.C., Enos M.D., Weis W.I., Garcia K.C. and Kobilka B.K. (2013) Adrenaline-activated structure of β2-adrenoceptor stabilized by an engineered nanobody. *Nature* **502**, 575-9.

Rodriguez D. and Gutierrez-de-Teran H. (2013) Computational approaches for ligand discovery and design in class-A G protein- coupled receptors. *Curr Pharm Des* **19**, 2216-36.

Rosenbaum D.M., Rasmussen S.G. and Kobilka B.K. (2009) The structure and function of G-protein-coupled receptors. *Nature* **459**, 356-63.

Rosenbaum D.M., Zhang C., Lyons J.A., Holl R., Aragao D., Arlow D.H., Rasmussen S.G., Choi H.J., Devree B.T., Sunahara R.K., Chae P.S., Gellman S.H., Dror R.O., Shaw D.E., Weis W.I., Caffrey M., Gmeiner P. and Kobilka B.K. (2011) Structure and function of an irreversible agonist-β2 adrenoceptor complex. *Nature* **469**, 236-40.

Scheerer P., Park J.H., Hildebrand P.W., Kim Y.J., Krauss N., Choe H.W., Hofmann K.P. and Ernst O.P. (2008) Crystal structure of opsin in its G-protein-interacting conformation. *Nature* **455**, 497-502.

Shi L. and Javitch J.A. (2004) The second extracellular loop of the dopamine D2 receptor lines the binding-site crevice. *Proc Natl Acad Sci U S A* **101**, 440-5.

Shim J.Y., Ahn K.H. and Kendall D.A. (2013) Molecular basis of cannabinoid CB1 receptor coupling to the G protein heterotrimer Gαiβγ: identification of key CB1 contacts with the C-terminal helix α5 of Gαi. *J Biol Chem* **288**, 32449-65.

Standfuss J., Edwards P.C., D'Antona A., Fransen M., Xie G., Oprian D.D. and Schertler G.F. (2011) The structural basis of agonist-induced activation in constitutively active rhodopsin. *Nature* **471**, 656-60.

Stevens R.C., Cherezov V., Katritch V., Abagyan R., Kuhn P., Rosen H. and Wuthrich K. (2013) The GPCR Network: a large-scale collaboration to determine human GPCR structure and function. *Nat Rev Drug Discov* **12**, 25-34.

Thompson M.D., Siminovitch K.A. and Cole D.E. (2008) G protein-coupled receptor pharmacogenetics. *Methods Mol Biol* **448**, 139-85.

Vaidehi N., Bhattacharya S. and Larsen A.B. (2014) Structure and dynamics of G-protein coupled receptors. *Adv Exp Med Biol* **796**, 37-54.

Venkatakrishnan A.J., Deupi X., Lebon G., Tate C.G., Schertler G.F. and Babu M.M. (2013) Molecular signatures of G-protein-coupled receptors. *Nature* **494**, 185-94.

Warne T., Serrano-Vega M.J., Baker J.G., Moukhametzianov R., Edwards P.C., Henderson R., Leslie A.G., Tate C.G. and Schertler G.F. (2008) Structure of a β1-adrenergic G-protein-coupled receptor. *Nature* **454**, 486-91.

Waugh D.J., Gaivin R.J., Zuscik M.J., Gonzalez-Cabrera P., Ross S.A., Yun J. and Perez D.M. (2001) Phe-308 and Phe-312 in transmembrane domain 7 are major sites of α1-adrenergic receptor antagonist binding. Imidazoline agonists bind like antagonists. *J Biol Chem* **276**, 25366-71.

Zeng F.Y., Soldner A., Schoneberg T. and Wess J. (1999) Conserved extracellular cysteine pair in the M3 muscarinic acetylcholine receptor is essential for proper receptor cell surface localization but not for G protein coupling. *J Neurochem* **72**, 2404-14.

Zhao M.M., Gaivin R.J. and Perez D.M. (1998) The third extracellular loop of the α2-adrenergic receptor can modulate receptor/G protein affinity. *Mol Pharmacol* **53**, 524-9.

Zhao M.M., Hwa J. and Perez D.M. (1996) Identification of critical extracellular loop residues involved in α1-adrenergic receptor subtype-selective antagonist binding. *Mol Pharmacol* **50**, 1118-26.

Zhou H. and Tai H.H. (2000) Expression and functional characterization of mutant human CXCR4 in insect cells: role of cysteinyl and negatively charged residues in ligand binding. *Arch Biochem Biophys* **373**, 211-7.

Molecular Pharmacology Fast Forward. Published on October 28, 2014 as DOI: 10.1124/mol.114.094557
This article has not been copyedited and formatted. The final version may differ from this version.

FOOTNOTES

This work was supported by an Australian NHMRC Project Grant [011246], an NHMRC Program Grant [569927] and an NHMRC Principal Research Fellowship [1019761].

Molecular Pharmacology Fast Forward. Published on October 28, 2014 as DOI: 10.1124/mol.114.094557
This article has not been copyedited and formatted. The final version may differ from this version.

FIGURE LEGENDS

Fig. 1. Structure and ECS of the α_{1B}-AR. (**A**) Top view of the α_{1B}-AR showing the backbone for mutated ECS in green, with the disulfide bond between ECL2 and TMH3 in yellow. The cleft between extracellular loop 2 (ECL2) and transmembrane helix 6 and 7 (TMH6 and TMH7) where agonists access the orthosteric binding site is further illustrated in B. (**B**) Top view of the α_{1B}-AR in the same orientation as A, with the surface of ECS residues colored by type, with nonpolar side chains in white, polar side chains in green, positively charged side chains in red and negatively charged side chains in blue. Non-ECS residues are shown in yellow.

Fig. 2. Effect of α_{1B}-AR mutants on NE EC_{50} in response to NE. Comparison of NE EC_{50} values for WT and α_{1B}-AR mutants measuring IP_1 accumulation in response to increasing concentrations of NE in transiently transfected COS-1 cells. Values are means ± SEM of 38 separate experiments for WT and 3–4 separate experiments for each mutants (each performed in triplicate). Determining the E_{max} values for IP_1 accumulation by α_{1B}-AR mutants revealed only the C118A mutant significantly reduced E_{max} versus the WT receptor (see Table 1).

Fig. 3. Effect of α_{1B}-AR mutants on NE K_i in response to NE. Comparison of NE K_i values for WT and α_{1B}-AR mutants. The affinity of NE at the WT receptor and α_{1B}-AR mutants were determined from displacement of the radiolabelled α_1-AR antagonist ^{3}H-prazosin (0.5 nM), or ^{125}I-(±)β-(iodo-4-hydroxyphenyl)-ethyl-aminomethyl-tetralone (^{125}I-HEAT; 70 pM) for the C195A mutant, using membranes from α_{1B}-AR-transfected COS-1 cells (5 µg protein) and increasing concentrations of NE. Values are means ± SEM of 10 separate experiments for WT and 2–3 separate experiments for each mutant (each performed in triplicate).

Fig. 4. Signaling efficiency (efficacy) of α_{1B}-AR mutants in response to NE. To characterize how effectively NE activated WT and mutant receptors, the NE efficacy was calculated as the NE pEC_{50} value minus the NE K_i value ($pEC_{50} - pK_i$) for NE at WT and α_{1B}-AR mutants (C118A mutant efficacy adjusted for decreased expression, see Table 1). Values are means ± SEM of 10 separate experiments for WT and 3 separate experiments for each mutant (each performed in triplicate).

Molecular Pharmacology Fast Forward. Published on October 28, 2014 as DOI: 10.1124/mol.114.094557
This article has not been copyedited and formatted. The final version may differ from this version.

Fig. 5. Effect of reduced expression levels on NE potency. A representative NE concentration response curve measuring IP_1 accumulation fitted with the operational model for WT α_{1B}-ARs at four different levels of expression (filled squares (■) 1x, filled circles (●) 0.3x, open squares (□) 0.1x, and open circles (○) 0.03x the standard (6 □g) DNA transfection). The average global K_A for NE was 6.94 ± 0.33 M (n = 3). The inset graph shows the relationship between log(B_{max}) and log(τ), which was fitted by linear regression (r^2 = 0.67, slope 1.8 ± 0.4) (data are means ± SEM of 3 separate experiments, each performed in triplicate).

Fig. 6. Structure of the ECS of the α_{1B}-AR showing key residues involved in NE affinity and/or efficacy. (A) Top view of the α_{1B}-AR ECS showing side chains for residues where mutations to alanine significantly changed NE K_i (red), NE efficacy (blue) or both NE K_i and efficacy (magenta) compared with WT α_{1B}-AR. The backbone of ECS residues without effect are coloured cyan. (**B**) Mutants that significantly changed NE K_i (red), NE efficacy (blue) or both NE K_i and efficacy (magenta) compared with WT α_{1B}-AR, with < 10-fold increased (↑) or decreased (↓), 10−100-fold decreased (↓↓), or 100−1000-fold decreased (↓↓↓) responses indicated.

Fig. 7. Functional heat map of the ECS of the α_{1B}-AR highlighting the position of mutations that influenced NE potency, affinity and efficacy. (A, C, E) Top view of the α_{1B}-AR showing the backbone for mutated ECS residues that significantly affected **(A)** NE potency (EC_{50}), **(C)** NE affinity (K_i), or **(E)** NE efficacy compared with WT α_{1B}-AR, orientated as shown in Fig. 1. (**B, D, F**) Top view of the α_{1B}-AR in the same orientation, showing the ECS with residues that significantly affected **(B)** NE potency (EC_{50}), **(D)** NE affinity (K_i), or **(F)** NE efficacy compared with WT α_{1B}-AR. Mutations causing < 10-fold increases (red) or decreases (light blue), 10−100-fold decreases (blue), or 100−1000-fold decreases (purple) are highlighted. Mutations at the ECS residues without effect are coloured white and non-ECS residues are shown in yellow.

Fig. 8. Sequence alignments for the ECS residues of selected Class A GPCRs. The hamster α_{1B}-AR and human α_{1B}-AR, α_{1A}-AR, α_{1D}-AR, α_{2A}-AR, β_1-AR, β_2-AR, muscarinic M2 and M3 receptor, dopamine D3 receptor, histamine H1 receptor and κ-opioid receptors were aligned using Clustal

Molecular Pharmacology Fast Forward. Published on October 28, 2014 as DOI: 10.1124/mol.114.094557
This article has not been copyedited and formatted. The final version may differ from this version.

Omega. The bars show the degree of conservation of residues determined using UGENE, with filled squares (■) indicating altered affinity and open circles (○) indicating altered efficacy determined from this study. The numbering represents the hamster α_{1B}-AR sequence and includes all residues mutated in this study.

Molecular Pharmacology Fast Forward. Published on October 28, 2014 as DOI: 10.1124/mol.114.094557
This article has not been copyedited and formatted. The final version may differ from this version.

Table 1. Pharmacological characterization of WT and mutant α_{1B}-ARs showing B_{max} determined from saturation binding assays, NE K_i determined from radioligand binding assays, NE EC_{50} and E_{max} determined measuring IP_1 accumulation in response to increasing concentrations of NE in an IP-one HTRF assay, with NE efficacy = $pEC_{50} - pK_i$.

Mutant	B_{max} % of WT	NE EC_{50}, nM	NE E_{max} % of WT	NE Ki, uM	NE Efficacy (log scale)
α_{1B} WT	100	11.9 ± 0.6 (38)	100	19.5 ± 1.8 (10)	3.22 ± 0.14 (10)
V107A	64.3 ± 3.8 (3)	11.6 ± 1.5 (3)	96.6 ± 3.6 (3)	7.9 ± 0.6 (3)*	2.83 ± 0.21 (3)
L108A	215.0 ± 15.0 (3)	5.8 ± 0.5 (3)	105.7 ± 7.4 (3)	26.5 ± 1.2 (3)	3.66 ± 0.12 (3)
G109A	49.7 ± 11.9 (3)	13.7 ± 1.7 (3)	93.0 ± 7.9 (3)	6.7 ± 1.0 (3)*	2.69 ± 0.27 (3)
Y110A	52.3 ± 9.6 (3)	37.7 ± 2.3 (3)*	99.3 ± 13.2 (3)	29.7 ± 1.6 (3)	2.90 ± 0.11 (3)
W111A	137.7 ± 32.3 (3)	129.22 ± 17.1 (3)*	83.9 ± 3.6 (3)	116.6 ± 3.7 (3)*	2.96 ± 0.16 (3)
V112A	305.7 ± 55.7 (3)	9.1 ± 1.0 (3)	99.0 ± 6.0 (3)	39.8 ± 1.3 (3)	3.64 ± 0.14 (3)
L113A	198.7 ± 41.1 (3)	136.6 ± 6.1 (3)*	126.3 ± 9.7 (3)	25.3 ± 1.3 (3)	2.27 ± 0.10 (3)*
G114A	56.0 ± 11.2 (3)	188.2 ± 9.5 (3)*	111.3 ± 7.5 (3)	16.9 ± 1.3 (3)	1.95 ± 0.13 (3)*
R115A	105.0 ± 16.0 (3)	121.9 ± 15.5 (3)*	95.8 ± 7.2 (3)	52.9 ± 3.9 (3)*	2.64 ± 0.20 (3)
I116A	238.3 ± 46.0 (3)	5.1 ± 0.7 (3)	98.8 ± 9.0 (3)	12.5 ± 0.9 (3)	3.39 ± 0.21 (3)
C118A	11.3 ± 3.5 (3)*	11134 ± 134 (3)*	53.0 ± 6.4 (3)*	518.8 ± 93.6 (3)*	1.67 ± 0.19 (3)*
P180A	148.0 ± 36.7 (3)	3983 ± 184 (4)*	64.3 ± 6.0 (4)	436.5 ± 8.7 (3)*	2.04 ± 0.07 (3)*
L181A	161.5 ± 82.5 (2)	241.6 ± 24.8 (4)*	96.5 ± 4.2 (3)	60.7 ± 2.7 (3)*	2.40 ± 0.15 (3)*
L182A	119.0 ± 81.0 (2)	21.8 ± 2.9 (3)	95.0 ± 10.2 (3)	22.1 ± 0.9 (3)	3.00 ± 0.17 (3)
G183A	349.7 ± 151.9 (3)	3280.6 ± 312.4 (4)*	65.9 ± 7.3 (4)	2398.8 ± 136.4 (3)*	2.86 ± 0.15 (3)
W184A	77.0 ± 16.0 (2)	395.1 ± 24.1 (3)*	97.1 ± 8.9 (3)	354.8 ± 19.5 (3)*	2.95 ± 0.12 (3)
K185A	131.5 ± 39.5 (2)	310.6 ± 18.9 (3)*	85.5 ± 4.6 (3)	187.6 ± 13.6 (3)*	2.78 ± 0.13 (3)
E186A	50.3 ± 18.7 (3)	156.1 ± 12.2 (3)*	100.7 ± 11.5 (3)	129.8 ± 10.9 (3)*	2.92 ± 0.16 (3)
P187A	118.3 ± 40.0 (3)	17.0 ± 3.2 (3)	84.0 ± 14.6 (3)	14.8 ± 1.6 (3)	2.94 ± 0.30 (3)
P189A	162.7 ± 59.4 (3)	59.7 ± 11.3 (3)*	104.2 ± 12.3 (3)	41.4 ± 3.5 (3)	2.84 ± 0.27 (3)
N190A	77.0 ± 7.0 (2)	475.4 ± 40.4 (4)*	86.4 ± 10.7 (3)	78.2 ± 4.6 (3)*	2.22 ± 0.14 (3)*
D191A	119.0 ± 47.0 (2)	52.0 ± 4.2 (3)*	87.5 ± 6.9 (3)	53.3 ± 0.9 (3)*	3.01 ± 0.10 (3)
D192A	89.7 ± 29.5 (3)	21.1 ± 2.6 (3)	80.5 ± 5.2 (3)	45.0 ± 5.7 (3)*	3.33 ± 0.25 (3)
K193A	89.0 ± 34.0 (2)	16.3 ± 0.1 (3)	97.0 ± 9.1 (3)	12.8 ± 1.1 (3)	2.89 ± 0.09 (3)
E194A	120.8 ± 19.7 (4)	11.6 ± 1.3 (3)	93.0 ± 13.8 (3)	35.2 ± 2.1 (3)	3.48 ± 0.17 (3)
C195A	38.5 ± 25.5 (2)	17660 ± 1048 (5)*	104.0 ± 17.3 (5)	3440.9 ± 212.4 (3)*	2.29 ± 0.12 (3)*
G196A	80.0 ± 58.0 (2)	120.2 ± 20.9 (3)*	97.8 ± 10.0 (3)	27.5 ± 1.7 (3)	2.36 ± 0.23 (3)*
V197A	46.0 ± 27.0 (2)	72.5 ± 3.5 (3)*	85.6 ± 5.1 (3)	10.1 ± 1.1 (3)	2.14 ± 0.15 (3)*
T198A	112.8 ± 2.3 (4)	241.6 ± 37.8 (3)*	100.1 ± 9.8 (3)	229.1 ± 4.8 (3)*	2.98 ± 0.18 (3)
E199A	113.0 ± 58.0 (2)	17.3 ± 1.1 (3)	90.7 ± 6.1 (3)	16.6 ± 0.9 (3)	2.98 ± 0.12 (3)
E200A	56.0 ± 18.0 (2)	238.0 ± 42.8 (3)*	89.2 ± 7.2 (3)	103.1 ± 6.0 (3)*	2.64 ± 0.24 (3)
P201A	64.0 ± 33.0 (2)	23.6 ± 4.4 (3)	87.9 ± 5.9 (3)	32.4 ± 6.3 (3)	3.14 ± 0.38 (3)
F202A	134.0 ± 19.7 (4)	8.7 ± 0.2 (3)	89.4 ± 7.0 (3)	23.8 ± 2.1 (3)	3.44 ± 0.11 (3)
L316A	113.5 ± 31.5 (2)	15.9 ± 0.5 (3)	94.3 ± 17.4 (3)	16.3 ± 1.0 (3)	3.01 ± 0.09 (3)
G317A	162.5 ± 43.5 (2)	52.8 ± 3.5 (3)*	95.2 ± 5.3 (3)	70.8 ± 5.4 (3)*	3.13 ± 0.14 (3)
S318A	170.5 ± 45.5 (2)	19.0 ± 3.2 (3)	75.2 ± 7.5 (3)	29.2 ± 1.9 (3)	3.18 ± 0.23 (3)
L319A	141.0 ± 61.0 (2)	14.6 ± 2.1 (3)	97.0 ± 11.6 (3)	35.2 ± 5.5 (3)	3.38 ± 0.30 (3)
F320A	163.0 ± 10.1 (4)	11.2 ± 1.6 (3)	98.1 ± 14.2 (3)	30.4 ± 2.9 (3)	3.44 ± 0.24 (3)
S321A	82.5 ± 10.5 (2)	11.6 ± 1.0 (3)	82.1 ±12.1 (3)	9.6 ± 0.4 (3)	2.92 ± 0.13 (3)
T322A	103.0 ± 1.0 (2)	12.5 ± 1.2 (3)	101.1 ± 14.3 (3)	9.1 ± 0.4 (3)	2.86 ± 0.14 (3)
L323A	176.8 ± 20.3 (4)	14.4 ± 1.2 (3)	83.4 ± 14.4 (3)	53.3 ± 2.5 (3)*	3.57 ± 0.13 (3)
K324A	59.0 ± 15.0 (2)	34.5 ± 4.0 (3)*	90.9 ± 3.9 (4)	17.3 ± 0.9 (3)	2.70 ± 0.17 (3)
P325A	113.0 ± 21.0 (2)	20.4 ± 2.0 (3)	93.1 ± 8.0 (3)	15.4 ± 1.1 (3)	2.88 ± 0.17 (3)
P326A	77.5 ± 5.5 (2)	39.7 ± 0.4 (3)*	83.6 ± 6.8 (3)	12.8 ± 0.2 (3)	2.51 ± 0.02 (3)
D327A	179.5 ± 51.5 (2)	6.9 ± 2.0 (3)	75.2 ± 8.7 (3)	9.6 ± 0.3 (3)	3.14 ± 0.32 (3)

Molecular Pharmacology Fast Forward. Published on October 28, 2014 as DOI: 10.1124/mol.114.094557
This article has not been copyedited and formatted. The final version may differ from this version.

V329A	86.3 ± 10.4 (4)	15.5 ± 1.2 (3)	101.5 ± 7.6 (3)	28.8 ± 2.8 (3)	3.27 ± 0.18 (3)
F330A	103.5 ± 40.5 (2)	38.5 ± 5.5 (3)*	86.6 ± 6.3 (3)	6.6 ± 0.5 (3)*	2.23 ± 0.22 (3)*
K331A	44.5 ± 27.5 (2)	9.9 ± 1.2 (3)	88.2 ± 9.3 (3)	2.1 ± 0.3 (3)*	2.33 ± 0.25 (3)*

Values are the mean ± SEM for the number of (*n*) separate experiments, * = signficant mutant effects compared to WT receptor

FIGURE 1

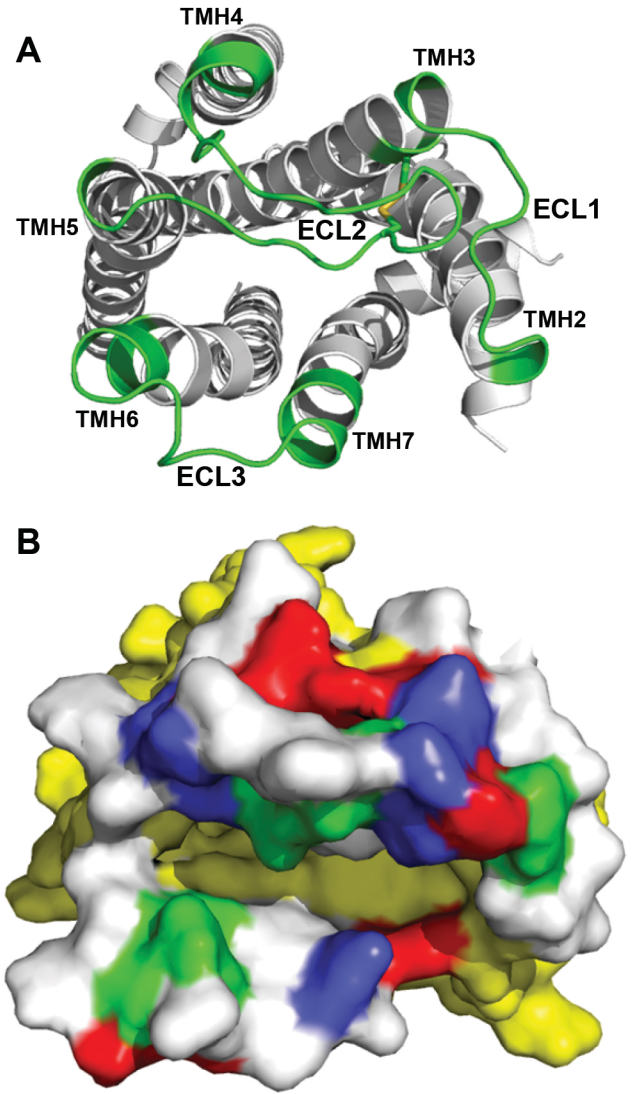

FIGURE 2

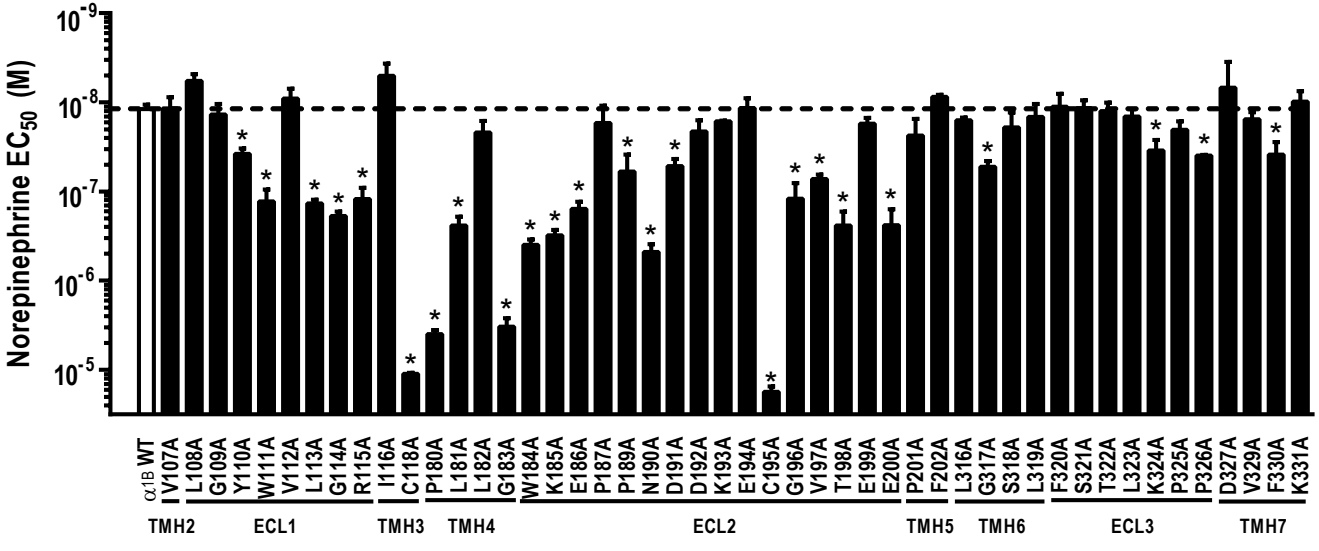
Norepinephrine EC50 (M)
10-9
10-8
10-7
10-6
10-5
α1B WT
V107A
L108A
G109A
Y110A
W111A
V112A
L113A
G114A
R115A
I116A
C118A
P180A
L181A
L182A
G183A
W184A
K185A
E186A
P187A
P189A
N190A
D191A
D192A
K193A
E194A
C195A
G196A
V197A
T198A
E199A
E200A
P201A
F202A
L316A
G317A
S318A
L319A
F320A
S321A
T322A
L323A
K324A
P325A
P326A
D327A
V329A
F330A
K331A
TMH2
ECL1
TMH3
TMH4
ECL2
TMH5
TMH6
ECL3
TMH7

FIGURE 3

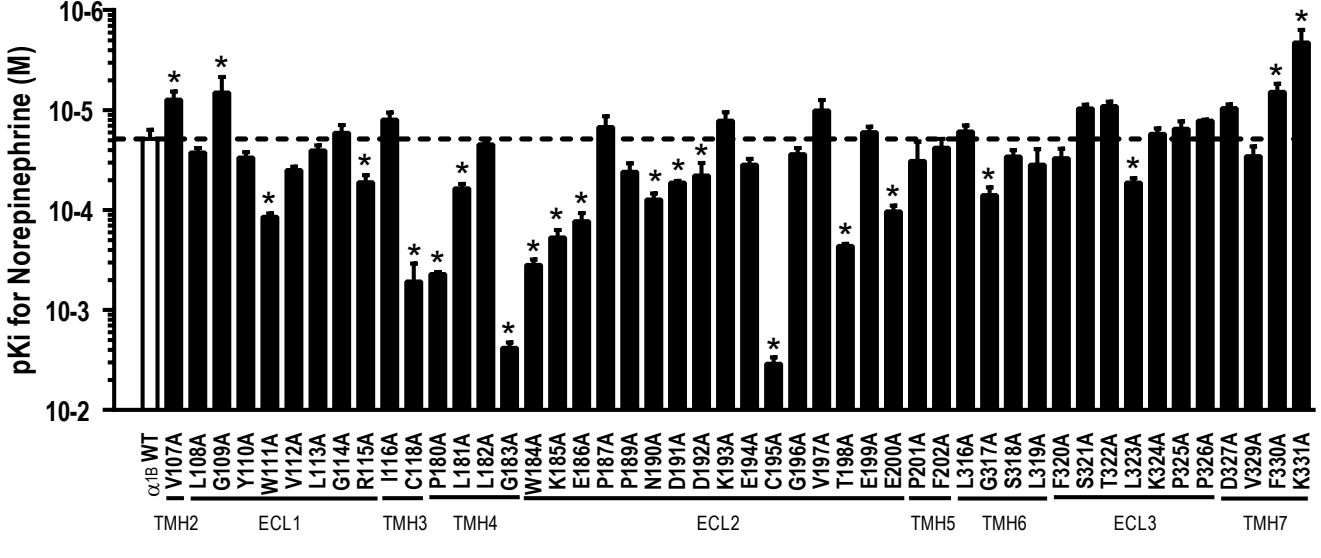
pKi for Norepinephrine (M)
10-6
10-5
10-4
10-3
10-2
α1B WT
V107A
L108A
G109A
Y110A
W111A
V112A
L113A
G114A
R115A
I116A
C118A
P180A
L181A
L182A
G183A
W184A
K185A
E186A
P187A
P189A
N190A
D191A
D192A
K193A
E194A
C195A
G196A
V197A
T198A
E199A
E200A
P201A
F202A
L316A
G317A
S318A
L319A
F320A
S321A
T322A
L323A
K324A
P325A
P326A
D327A
V329A
F330A
K331A
TMH2
ECL1
TMH3
TMH4
ECL2
TMH5
TMH6
ECL3
TMH7

FIGURE 4

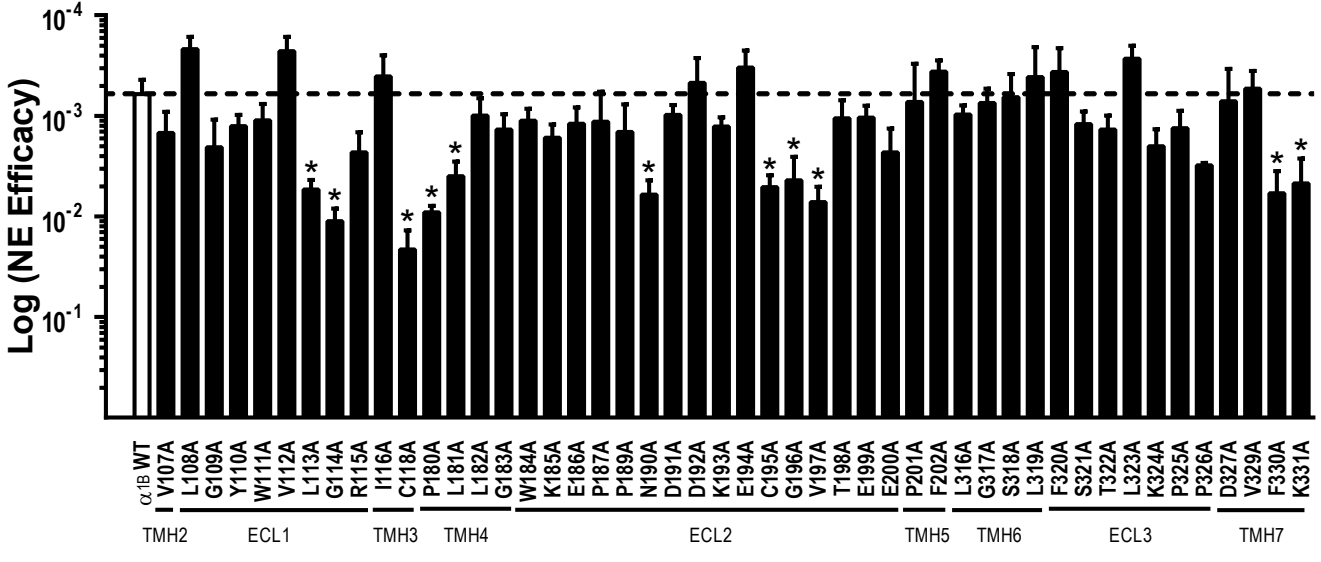
Log (NE Efficacy)
10-4
10-3
10-2
10-1
α1B WT
V107A
L108A
G109A
Y110A
W111A
V112A
L113A
G114A
R115A
I116A
C118A
P180A
L181A
L182A
G183A
W184A
K185A
E186A
P187A
P189A
N190A
D191A
D192A
K193A
E194A
C195A
G196A
V197A
T198A
E199A
E200A
P201A
F202A
L316A
G317A
S318A
L319A
F320A
S321A
T322A
L323A
K324A
P325A
P326A
D327A
V329A
F330A
K331A
TMH2
ECL1
TMH3
TMH4
ECL2
TMH5
TMH6
ECL3
TMH7

Figure 5

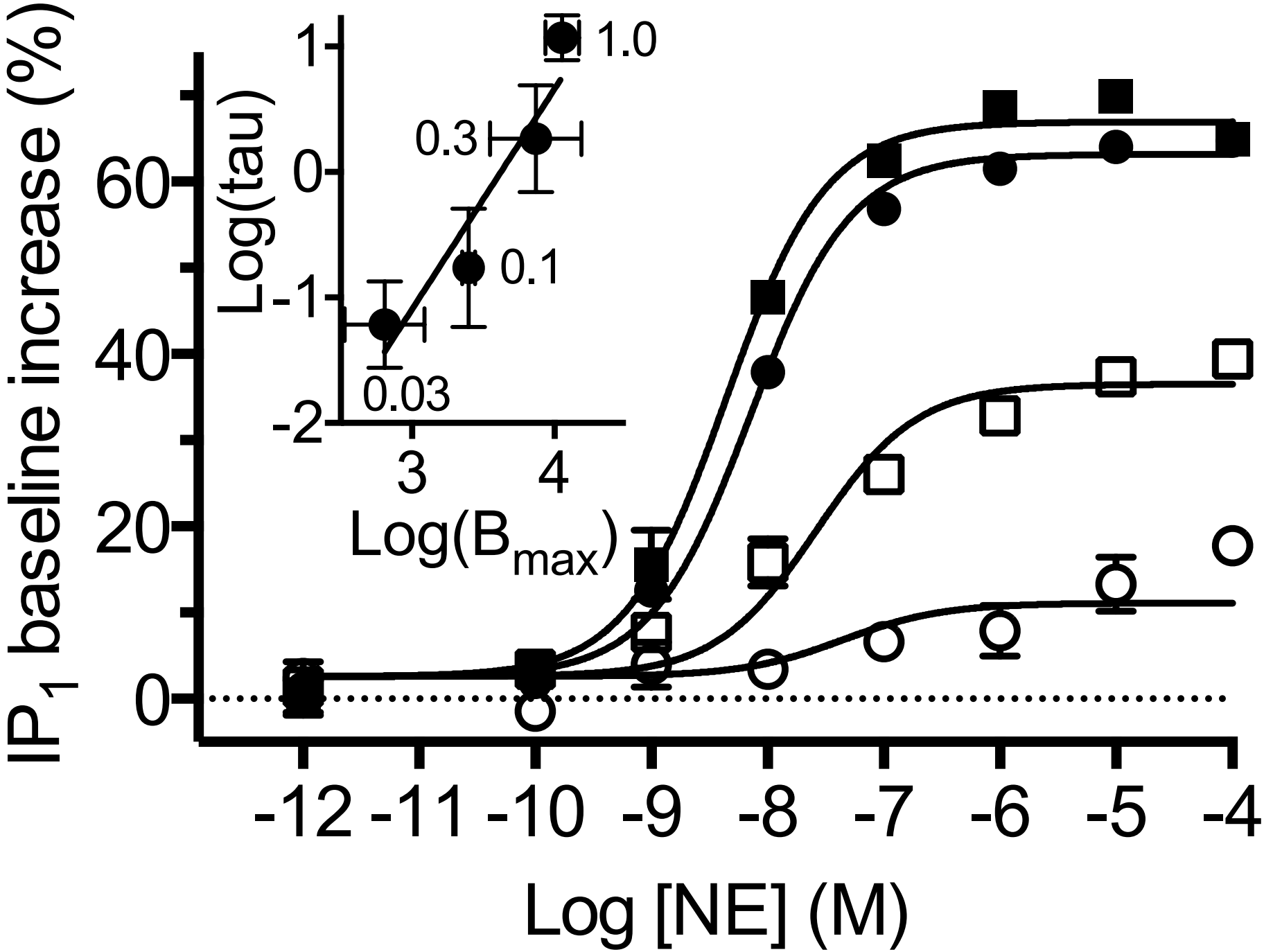
IP1 baseline increase (%)
60
40
20
0
-12 -11 -10 -9 -8 -7 -6 -5 -4
Log [NE] (M)
Log(tau)
1
0
-1
-2
1.0
0.3
0.1
0.03
3
4
Log(Bmax)

FIGURE 6

A

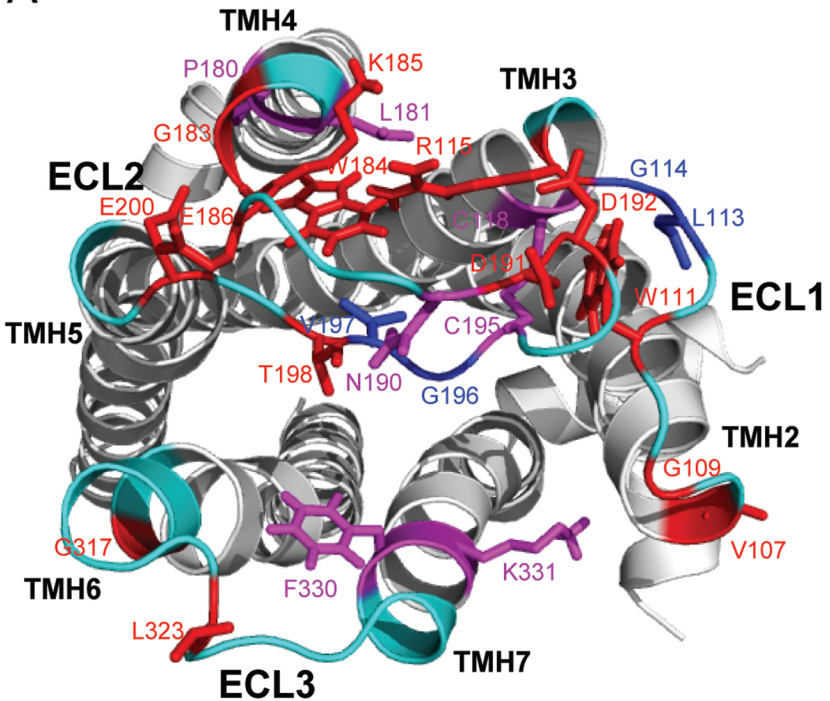

B

Mutant	Position	Affinity	Efficacy
V107A	TMH2	↑	
G109A	ECL1	↑	
W111A	ECL1	↓	
L113A	ECL1		↓
G114A	ECL1		↓↓
R115A	ECL1	↓	
C118A	TMH3	↓↓	↓↓
P180A	TMH4	↓↓	↓↓
L181A	TMH4	↓	↓
G183A	TMH4	↓↓↓	
W184A	ECL2	↓↓	
K185A	ECL2	↓↓	
E186A	ECL2	↓↓	
N190A	ECL2	↓	↓
D191A	ECL2	↓	
D192A	ECL2	↓	
C195A	ECL2	↓↓↓	↓
G196A	ECL2		↓
V197A	ECL2		↓↓
T198A	ECL2	↓↓	
E200A	ECL2	↓	
G317A	TMH6	↓	
L323A	ECL3	↓	
F330A	TMH7	↑	↓
K331A	TMH7	↑	↓

FIGURE 7

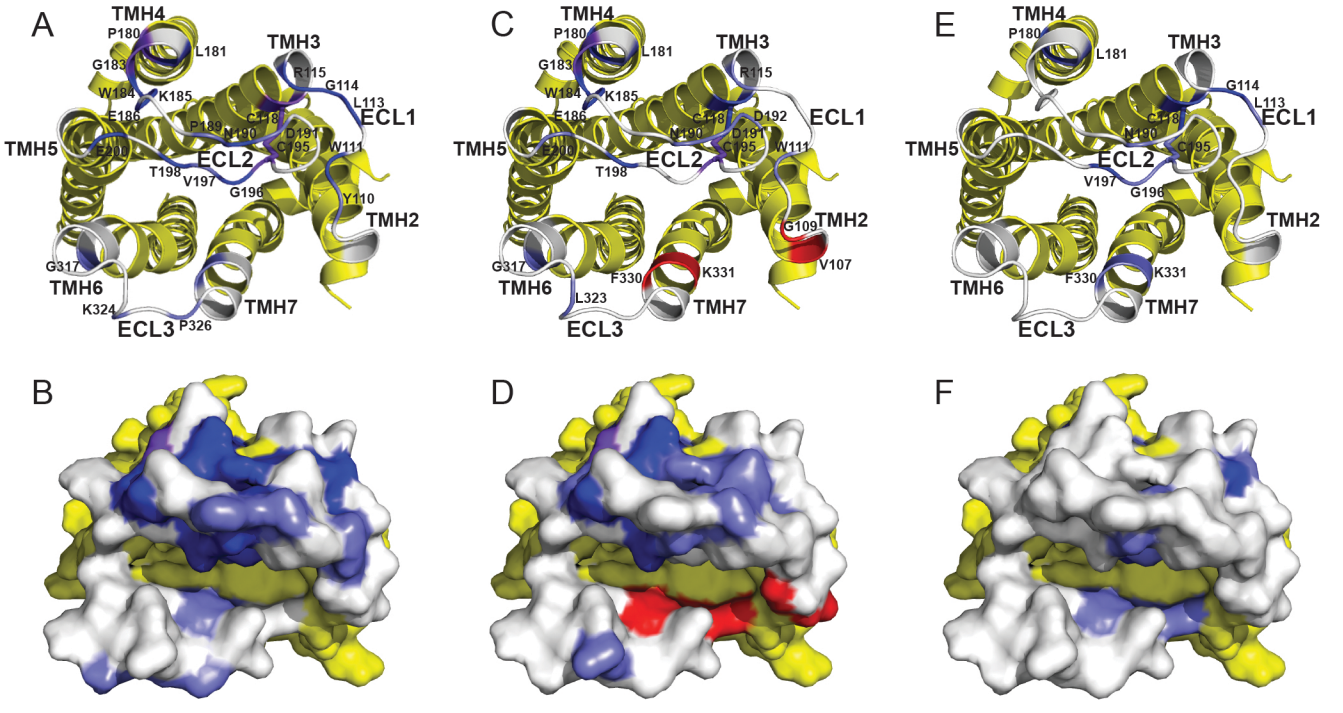
A
TMH4
P180
L181
G183
TMH3
R115
W184
K185
G114
L113
E186
ECL1
P189
N190
D191
TMH5
S200
ECL2
C195
W111
T198
V197
G196
Y110
TMH2
G317
TMH6
K324
TMH7
ECL3
P326
B
C
TMH4
P180
L181
G183
TMH3
R115
W184
K185
E186
ECL1
D192
N190
D191
TMH5
S200
ECL2
C195
W111
T198
G109
TMH2
V107
G317
F330
K331
TMH6
L323
TMH7
ECL3
D
E
TMH4
P180
L181
TMH3
G114
L113
ECL1
TMH5
N190
ECL2
C195
V197
G196
TMH2
F330
K331
TMH6
TMH7
ECL3
F

FIGURE 8

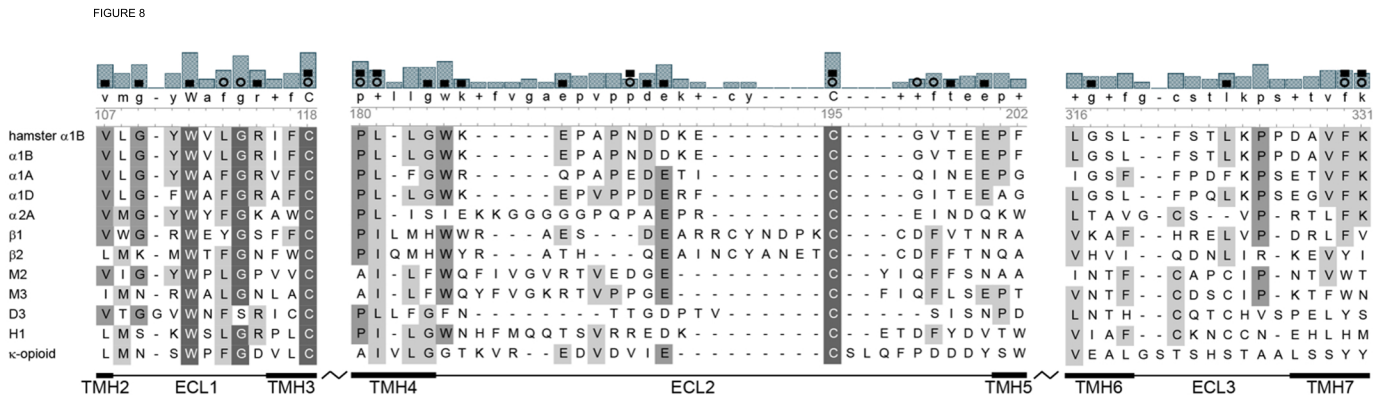
v m g - y W a f g r + f C
p + l l g w k + f v g a e p v p p d e k + - c y - - - - C - - - + + f t e e p +
+ g + f g - c s t l k p s + t v f k
107
118
180
195
202
316
331
hamster α1B
α1B
α1A
α1D
α2A
β1
β2
M2
M3
D3
H1
κ-opioid
TMH2
ECL1
TMH3
TMH4
ECL2
TMH5
TMH6
ECL3
TMH7